Welding in the World (2024) 68:155–162
https://doi.org/10.1007/s40194-023-01644-x

RESEARCH PAPER

Effect of post-welding heat treatment on microstructure and properties of electron beam welding joint of new high-strength TB18 titanium alloy

Jian Long[1] · Lin-Jie Zhang[1] · Long Zhang[2] · Miao-Xia Xie[2]

Received: 26 September 2023 / Accepted: 21 November 2023 / Published online: 30 November 2023

Abstract
This paper investigates the influence of post-weld heat treatment (PWHT) on the microstructure and mechanical properties of an 80-mm thick TB18 electron beam–welded (EBW) joint. The average tensile strength of TB18 base metal (BM) is 1328 MPa, while the tensile strength of as-welded joints is 736 MPa, which is only 55.3% of the BM. After post-welding heat treatment (PWHT), the tensile strength of the joint is slightly higher than that of the BM, which is 1341 MPa. The fracture morphology of the BM and two kinds of joints are analyzed. There are a lot of dimples in the tensile fracture of the BM and as-welded joint, which are ductile fractures, while the tensile fracture morphology of the PWHT joint is mainly composed of dimples and cleavage planes, which are quasi-cleavage fractures. The microhardness of the weld metal (WM) of the as-welded joint is significantly lower than that of the BM, while the microhardness of the PWHT joint is close to that of the BM. There are obvious differences in the microstructure of the WM between the two kinds of joints. The WM of the as-welded joint is mainly composed of large β columnar crystals, while a large number of fine flaky α′ phases are precipitated in the WM of the PWHT joint.

Keywords Ti-4Al-5 V-5Mo-5Cr-1Nb (TB18) · Electron beam welding · Post-weld heat treatment · Microstructure

1 Introduction

The main high-strength titanium alloys are TC18, Ti1023, and Ti55531. The tensile strength of these titanium alloys after heat treatment can reach 1100 ~ 1200 MPa, and the fracture toughness can reach 50 ~ 60 MPa·m$^{1/2}$ [1–3]. These titanium alloys have both high tensile strength and good fracture toughness. Although the mechanical properties of these titanium alloys are relatively high, it is still difficult to meet the demand for ultra-high strength and high-toughness titanium alloys in the aviation field. In particular, the key-bearing components of aviation equipment, such as the bearing frame and beam on the fuselage. These structural parts play an important role in ensuring the development of aviation equipment.

The latest TB18 titanium alloy, a new type of near-β titanium alloy, has the characteristics of high tensile strength, good fracture toughness, large quenchability, etc. It is suitable for manufacturing large bearing components with high strength requirements and good weight reduction effect and is mainly used as important load parts such as aircraft landing gear and beam [4, 5]. Due to the large size of aviation structures, it is difficult to achieve overall forging. In order to achieve the connection of large-sized structural parts, welding technology is needed [6, 7]. The vacuum electron beam welding technology has the advantages of high energy density, small thermal input, small welding deformation, and good stability. It has been widely used in the fields of aerospace [8, 9]. Titanium alloy when welding is easy with the oxygen in the air, the reaction of impurities such as nitrogen and hydrogen, which makes the welding joint embrittlement. The vacuum electron beam welding (EBW) technology is welded in a vacuum environment, which avoids the reaction of titanium alloy molten metal with oxygen, hydrogen, water vapor, and other impurity gases in the environment during the welding process and can obtain better welding quality [10, 11].

Recommended for publication by Commission IV—Power Beam Processes.

✉ Lin-Jie Zhang
zhanglinjie@mail.xjtu.edu.cn

[1] State Key Laboratory for Mechanical Behavior of Materials, Xi'an Jiaotong University, Xi'an 710049, China

[2] School of Mechanical and Electrical Engineering, Xi'an University of Architecture and Technology, Xi'an 710055, China

At present, the main research on new titanium alloys is the relationship between the microstructure and mechanical properties of the material itself. Zhang et al. [12] studied the effects of laser power, scanning speed, and powder feeding rate on the TB18 titanium alloy microstructure and morphology of single-pass sediments and blocks, and optimized the forming process parameters. The results show that with the increase of scanning speed and laser power, and the decrease of powder feed rate, the aspect ratio of single passage deposition increases [12]. Zhou et al. [13] also studied the effects of heat treatment on the microstructure and mechanical properties of TB18. The results show that the microstructure is composed of β grains when the solution temperature is higher than 830 °C. After solution + aging, the secondary α phase precipitates, and the tensile strength and yield strength increase significantly, while the elongation decreases [13].

In summary, there are few reports on the weldability and welding joint PWHT of the new near-β titanium alloy TB18. In this paper, the effect of PWHT on microstructure and properties of high strength and toughness titanium alloy Ti-4Al-5 V-5Mo-5Cr-1Nb (TB18) EBW joint is studied, which includes five parts: The first part is the research background; the second part is the experimental

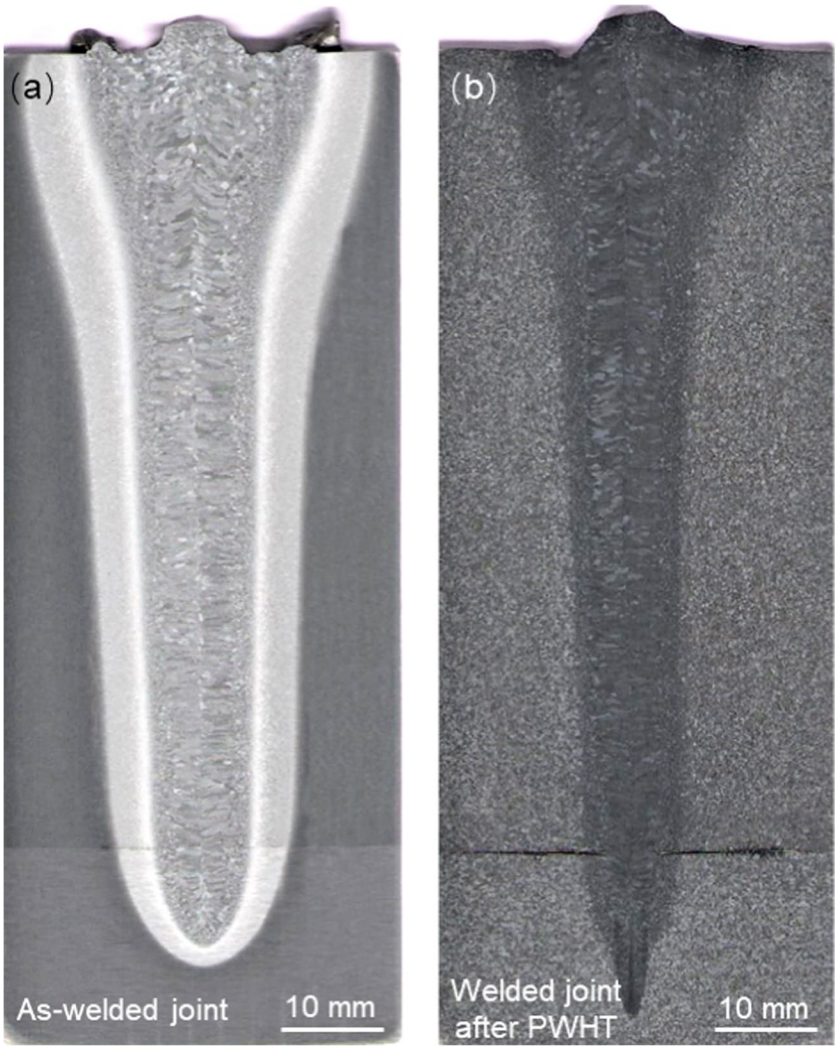

Fig. 1 Cross-section topography of two kinds of joints: **a** as-welded joint and **b** welded joint after PWHT

Table 1 Chemical compositions of TB18 titanium alloy (wt, %)

Material	Al	Mo	Nb	Cr	V	Fe
TB18	4.04	4.91	1.01	5.96	4.86	Balance

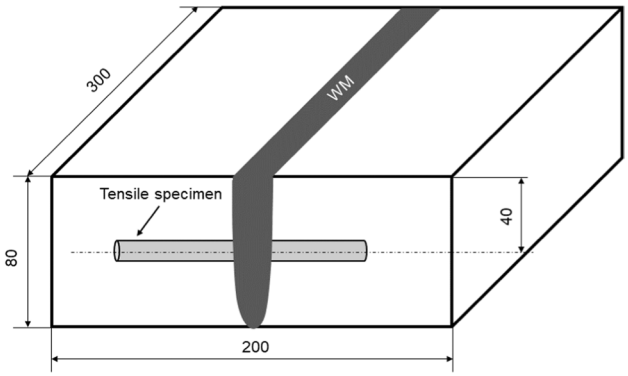

Fig. 2 Sampling position of tensile specimen

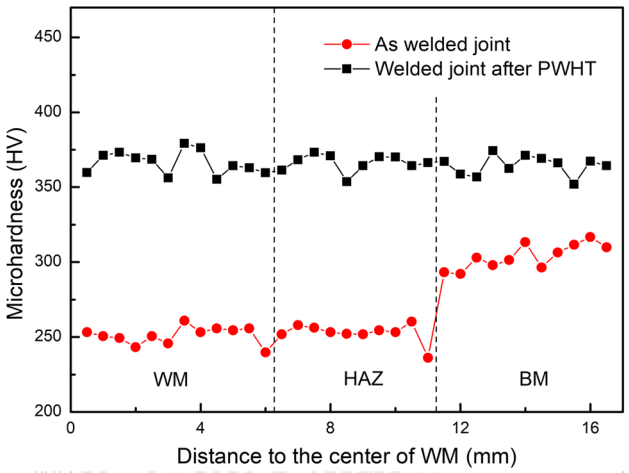

Fig. 4 Microhardness of each area of the two joints

materials and methods; the third part is the comparison of mechanical properties between PWHT joints and as-welded joints. The fourth part analyzes the reasons for the obvious improvement of joint strength. The microstructure of the joint was significantly improved by PWHT. The fifth part is the summary of the main experimental results.

2 Materials and methods

2.1 Materials

Figure 1a shows the cross-section morphology of TB18 as-welded joints. Figure 1b shows the cross-section morphology of the welded joint after PWHT. It can be seen from the figure that the center width of the weld is about 12.3 mm, and the width of the heat-affected zone is about 5.1 mm. After the test plate is welded, solid solution + aging treatment is performed, solid solution temperature is 870 °C, heat preservation is performed for 120 min, and then aging treatment is performed at 530 °C, heat preservation time is 240 min, and finally, air cooling is performed. Heat treatment was carried out in a vacuum environment. The welding part is made of two test plates with a length of 300 mm, a width of 100 mm, a thickness of 80 mm, and the thickness of the backing plate is 20 mm. Table 1 shows the chemical composition information of the materials.

2.2 Microstructure observation

The corrosion agent used in the test was Keller's reagent (HF to HNO_3 to H_2O = 1:3:50), and the corrosion time was about 10 s. The microstructures of BM, HAZ, and WM were observed under high resolution scanning electron microscope. The equipment model is FEI Verios460. The microstructures of BM and WM were observed under transmission electron microscopy. The experimental equipment model is JEM-2100F. When preparing the specimen for TEM observation, the specimen was first ground to about 30 μm with 2000-mesh silicon carbide sandpaper, and then thinned by twin-jet electrolytic spraying. The electrolyte was a methanol sulfate solution with a concentration of 8%.

2.3 Mechanical test

The micro-Vickers hardness curve is from the center of the weld to the right BM with a dot interval of 0.25 mm. The test equipment is HXD-1000TMC/LCD. The test force is 200 g (1.961 N) and the load holding time is 15 s. Microhardness was measured in the center of the plate thickness.

The tensile test was carried out on the INSTRON 1195 electronic tensile test machine at the speed of 0.5 mm/min. Figure 2 shows the sampling position of the tensile sample, and the size

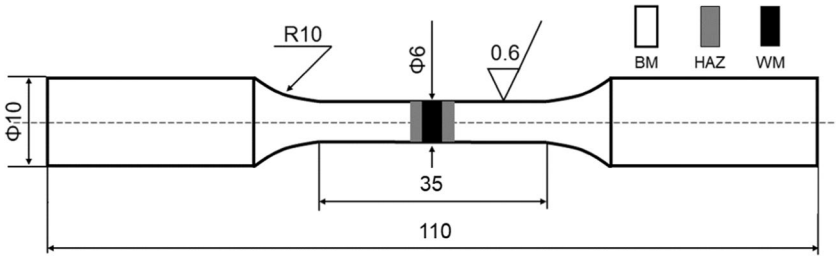

Fig. 3 The size of the tensile specimen

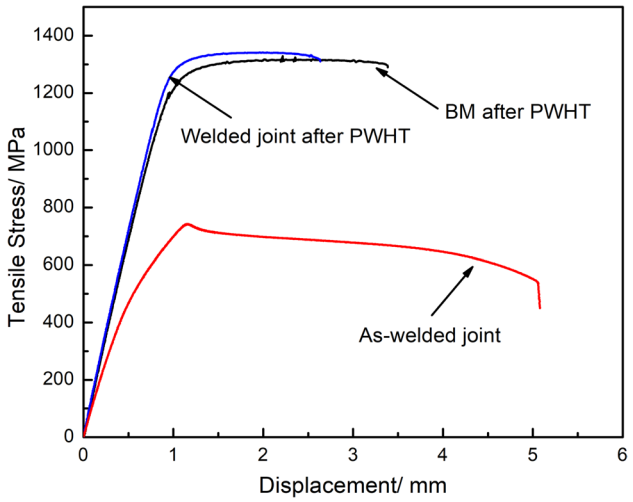

Fig. 5 Tensile curves of BM and two kinds of joints

diagram is shown in Fig. 3. The fracture of the tensile specimen was observed by scanning electron microscope (SU3500).

3 Results

3.1 Microhardness of each area of the two joints

Figure 4 shows the microhardness of 80 mm thick TB18 titanium alloy in each region of as-welded and PWHT joints. After PWHT, the average microhardness of each region of the TB18 EBW joint can be significantly improved. For as-welded joint. The average hardness values of WM, heat-affected zone (HAZ), and BM are 252HV, 251HV, and 303HV, respectively. After PWHT, the average values of WM, HAZ, and BM are 366HV, 362HV, and 361HV, respectively. For as-welded joints, the hardness values of WM and HAZ are close, but both are significantly lower than that of BM. The hardness of WM is about 17% lower than that of BM. The average microhardness values of the PWHT joint are very close to each other and are significantly higher than those of the as-welded joint. After PWHT, the WM, HAZ, and BM of TB18 EBW as-welded joint were increased by 114HV, 111HV, and 58HV, respectively.

3.2 Tensile properties of two types of joints

Figure 5 shows the tensile results of the as-welded joint and welded joint after PWHT and BM. The effect of post-welding heat treatment on joint strengthening is very obvious. The tensile strength of the BM is 1328 MPa, the tensile strength of the as-welded joint is 742 MPa, and the tensile strength of the welded joint after PWHT is 1341 MPa. The tensile strength of the joint is increased by 80.7% after the PWHT, which is as strong as the BM. The elongation of BM, as-welded and PWHT joints of TB18 titanium alloy is 9.6%, 14.4%, and 7.8%, respectively. Figure 6 shows the tensile fracture positions of the as-welded and PWHT joints of TB18 titanium alloy. It can be seen from the figure that the tensile samples of the two joints were broken in the WM.

Figure 7 shows the tensile fracture morphology of BM, as-welded joint, and PWHT joint. Figure 7a shows the full view of the tensile fracture of the BM. Figure 7d and g shows a partially enlarged view of the fracture. It can be seen from the figure that there are a large number of dimples in the BM, and the fracture mode is a ductile fracture. Figure 7b shows the overall picture of the tensile fracture of the as-welded joint. Figure 7e and h are partial enlargements of the as-welded joint. A large number of

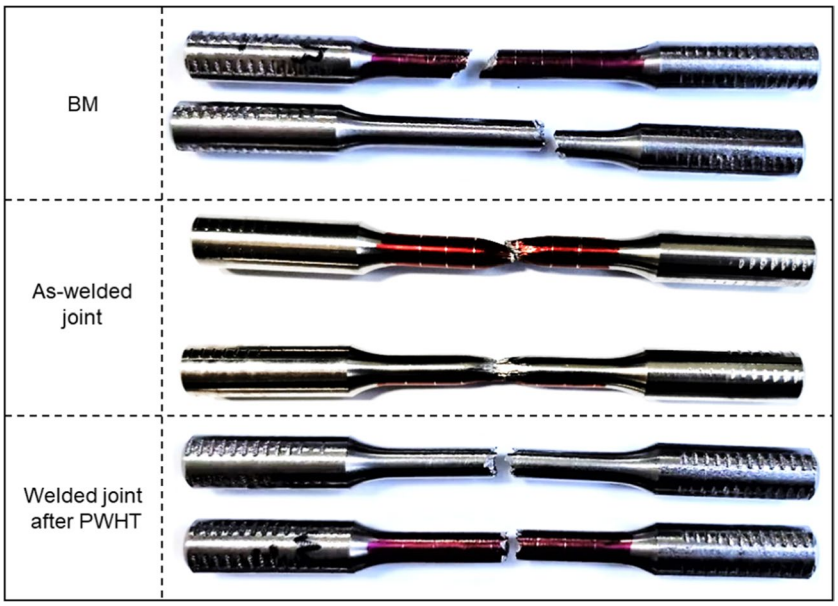

Fig. 6 Tensile fracture positions of BM, as-welded, and PWHT joint

dimples were also found in the fracture, and the fracture mode was also ductile fracture. Figure 7c shows the overall picture of the tensile fracture of the welded joint after PWHT. In Fig. 7f and i, there are flat "cleavage-like" facet planes and small dimples with shallow holes distributed in the fracture, and there are tearing edges at the edges of the dimples. Therefore, the fracture of a welded joint after PWHT is a quasi-cleavage fracture, and the fracture mode is a brittle fracture.

4 Discussion

4.1 Microstructure of the two joints

Figure 8 shows the microstructure of the BM, HAZ, and WM of as-welded and PWHT joints under high-resolution scanning electron microscopy (HR-SEM). Figure 8a shows the BM of the welded joint, which is mainly composed of the equiaxed α phase and β transition structure. Figure 8d is a local magnification of Fig. 8a showing the presence of strip α phases in the β-transition structure. Figure 8b shows the structure of the HAZ of the welded joint. It is found that the equiaxed α phase is still retained, and the β transition structure can be found dissolved in the matrix through Fig. 8e. Figure 8c shows the microstructure of the WM of the welded joint. The α phase has been completely transformed and is mainly composed of β grains. Figure 8f is a local enlargement of the microstructure of the WM, and it is found that the rivalent boundary of the WM is significantly larger than in other areas. As shown in reference [14, 15], the grain boundary in the crystal will hinder the movement of the dislocation, the grain size is large, the grain boundary is less,

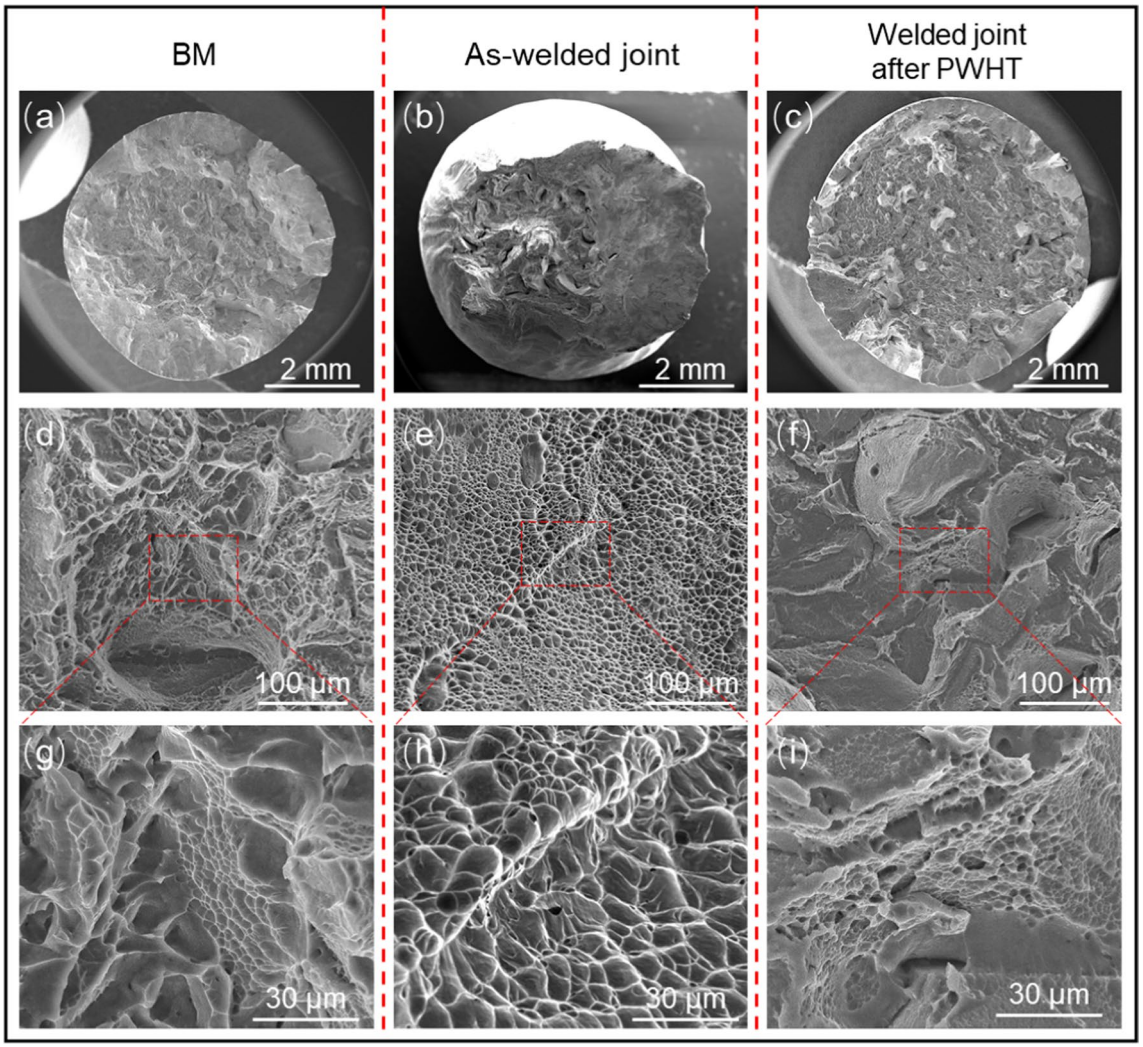

Fig. 7 Tensile fracture morphology of BM, as-welded, and PWHT joint. **a**, **b,** and **c** are the macro fracture morphology of BM, as-welded, and PWHT joints, respectively. **d**, **e,** and **f** are the local morphologies of BM, as-welded, and PWHT joints, respectively. **g**, **h,** and **i** are local enlargements of **d**, **e**, and **f**, respectively

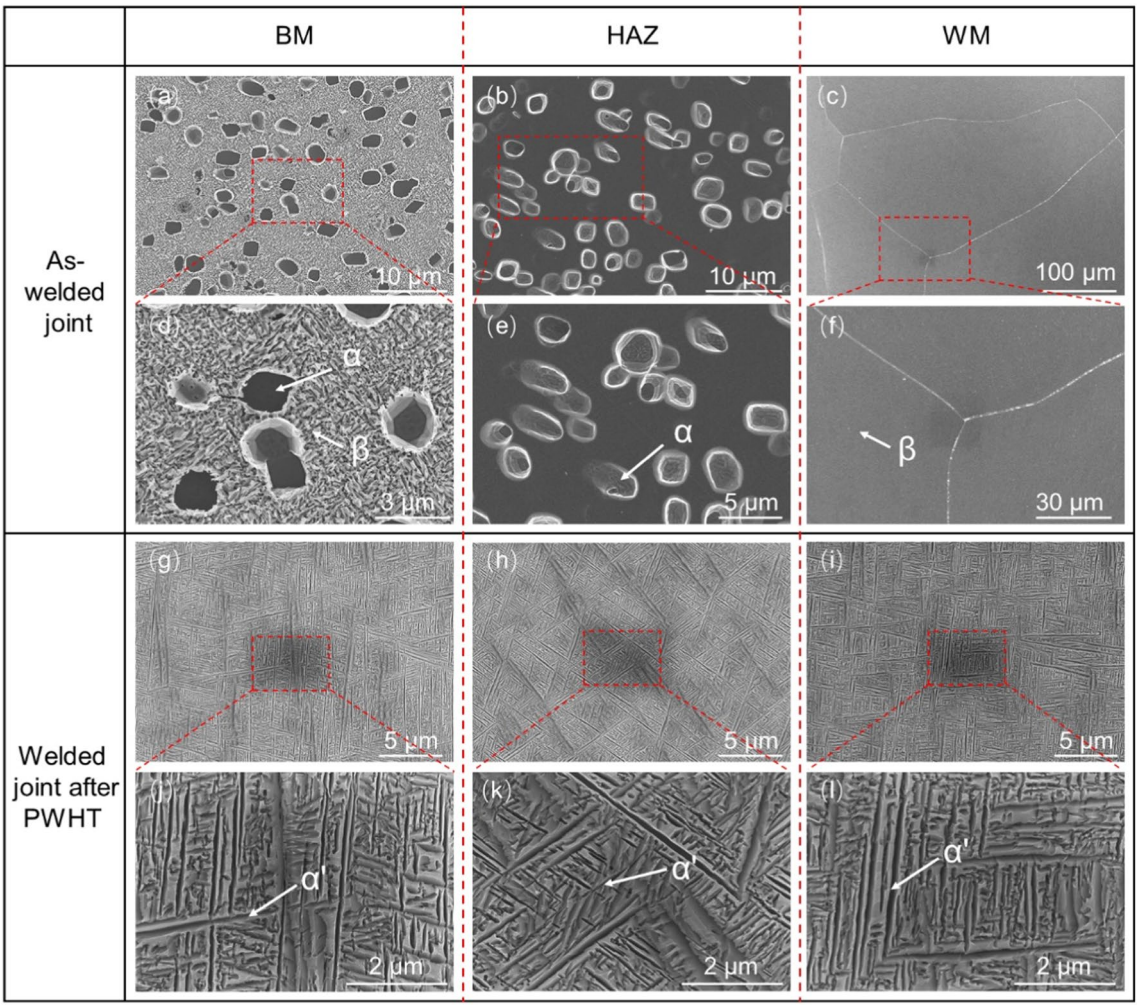

Fig. 8 Microstructure of each region of the two joints. **a**, **b**, and **c** are the microstructure of the base material, heat-affected zone, and weld zone of the as-welded joint, respectively. **d**, **e**, and **f** are local enlargements of **a**, **b**, and **c**, respectively; **g**, **h**, and **i** are the microstructure of the base metal, heat-affected zone, and weld zone of the PWHT joint, respectively. **j**, **k**, and **l** are local enlargements of **g**, **h**, and **i**, respectively

when the material is deformed, the resistance of the dislocation movement is small, and the strength is low, which is an important reason for the strength decline of the as-welded joint and the hardness of the WM.

Figure 8g and j shows the microstructure of the BM of the welded joint after PWHT. It can be observed that there are a large number of acicular secondary α′ phases in the β grain, and the acicular α′ phases are crisscrossed. Figure 8h and k shows the microstructure of the HAZ, which is similar to that of the BM, and a large number of secondary α′ phases are also found in this region. Figure 8i and l shows the microstructure of the WM. A large number of secondary α′ phases were also found in this area.

In a word, a large amount of acicular α′ phase is precipitated in each area of the welded joint after PWHT, which significantly improves the overall tensile strength of the joint.

4.2 TEM analysis on joints

Figure 9 shows the microstructure of the BM and WM of the two kinds of joints under TEM. Figure 9a shows the morphology of the BM of the as-welded joint, in which the equiaxed α phase and fine acicular α′ phase are found. Figure 9b shows the morphology of the BM of the welded joint after PWHT, all of which show that there are acicular α′ phases distributed on the β matrix. Studies have shown that [16, 17] in high-strength titanium alloys, the acicular α′ phase as the reinforcing phase can significantly improve the strength of titanium alloys. Figure 9c shows the microstructure of the WM of the as-welded joint. It is found that the reinforcement phase has dissolved and a small number of dislocation lines can be observed. Figure 9d shows the microstructure of the WM of the welded joint after PWHT. Through solution aging, the acicular α′ phase is re-precipitated, and a

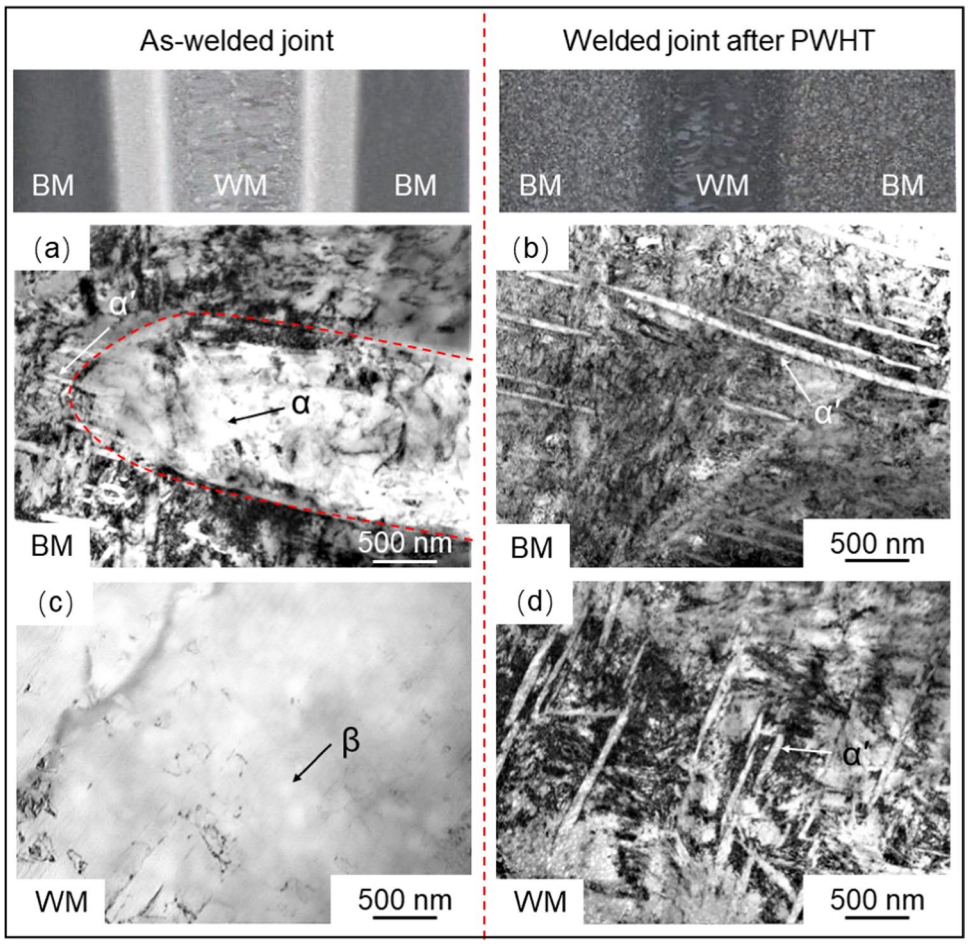

Fig. 9 Microstructures in the BM and WM of the two kinds of joints. **a** is the microstructure of the base material of the as-welded joint; **b** is the weld microstructure of the as-welded joint; **c** is the microstructure of the base metal of the PWHT joint; and **d** is the weld microstructure of the PWHT joint

large number of dislocation entanglement occurs at the same time. Studies have shown [18, 19] that the dislocation in the matrix will interact with the new dislocation generated by the deformation of the material so that the dislocation will wind and gather, and greater external force is required to make the dislocation continue to move, thus improving the strength of the material, which is also an important reason for the strength of the welded joint after PWHT.

5 Conclusions

The mechanical properties of high strength and toughness titanium alloy TB18 EBW joint of as-welded joint and welded joint after PWHT were studied. There are main conclusions shown as follows:

(1) Through PWHT, the tensile strength of the joint is significantly improved. The tensile strength of the as-welded joint is 742 MPa, and the welded joint after PWHT is 1341 MPa.
(2) After PWHT, the microhardness of each area of the joint is significantly improved. Compared with the as-welded joint, the average microhardness of WM, HAZ, and BM of the joint increased by 114 HV, 111 HV, and 58 HV, respectively.
(3) Through PWHT, a large number of reinforcement phases are precipitated in the WM. The reinforced phase in the WM of the as-welded joint dissolved in the β matrix, while a large number of fine flaky α′ phases were re-precipitated in the WM of the welded joint after PWHT.
(4) After PWHT, the dislocation density in the WM increases. Only a small amount of dislocation lines were observed in the WM of the as-welded joint, while a large number of dislocation entanglement appeared in the WM of the welded joint after PWHT.

Acknowledgements The authors would thank the teachers at the Instrument Analysis Center of Xi'an Jiaotong University for their assistance with SEM analysis. Thanks to Shan-Lin Zhou and Chuan-Wei Fan from the School of Materials Science and Engineering of Xi'an Jiaotong University for their help in the experimental part of the paper.

Author contribution Lin-Jie Zhang and Jian Long contributed to the conception of the study. Jian Long contributed significantly to the analysis, manuscript preparation, and conduct of the experiment.

Long Zhang helped perform the analysis with constructive discussions. Miao-Xia Xie provided constructive suggestions to improve the manuscript.

Funding This work was supported by the National Natural Science Foundation of China (grant no. 51775416), the National Thousand Talents Program of China (grant no. WQ2017610446), and the Project of Innovation Team of Xi'an Jiaotong University (grant no. XTR0118008).

Data availability The data that support the findings of this study are available from the corresponding author [Zhang L-J], upon reasonable request.

Data and code availability The raw/processed data required to reproduce these findings cannot be shared at this time as the data also forms part of an ongoing study.

Declarations

Ethics approval and consent to participate There are no experiments involving human tissue.

Conflict of interest The authors declare no competing interests.

References

1. Yan M, Sha A, Zhang W et al (2015) Recovery and recrystallization behavior of large sized β phase grains in TC18 titanium alloy during annealing process [J]. Mater Sci Forum 817:263–267
2. Ru-Qiang B, Xu H, Chun-Xiao C (2006) Deformation behavior and mechanisms of Ti-1023 alloy [J]. Trans Nonferrous Metals Soc China 16(002):274–280
3. Long J, Zhang LJ, Ning J et al (2021) Effects of post-weld heat treatment on microstructures and properties of laser welded joints of new high-strength Ti-55531 alloy [J]. J Manuf Process 64:1329–1335
4. Fu Q, Yuan W, Xiang W (2021) Dynamic softening mechanisms and microstructure evolution of TB18 titanium alloy during uniaxial hot deformation [J]. Metals - Open Access Metall J 11(5):789
5. Fu Q, Yuan W, Xiang W (2020) Constitutive relationship for hot deformation of TB18 titanium alloy [J]. Adv Mater Sci Eng. https://doi.org/10.1155/2020/5716548
6. Samelor D, Baggetto L, Laloo R et al (2020) Efficient, durable protection of the Ti6242S titanium alloy against high-temperature oxidation through MOCVD processed amorphous alumina coatings [J]. J Mater Sci 55(11):4883–4895
7. Luo J-m, Chen Y-h, Huang J, Xu J-l (2019) Effect of shot peening and micro-arc oxidation on microstructure and fatigue properties of TC4 titanium alloy [J]. Chin J Nonferrous Metals 29(6):1210–18
8. Long J, Zhang L-J, Zhang L-L, Ning J, Zhuang M-X, Zhang J-X et al (2021) Analysis of heterogeneity of fatigue properties of double-sided electron beam welded 140-mm thick TC4 titanium alloy joints [J]. Int J Fatigue 142:105942
9. Gao Q, Jiang P, Geng Y, Gao F, Yu W (2020) Microstructure and properties of electron beam welded joint for Ti-6321 large thickness titanium alloy [J]. Rare Metal Mater Eng 49(3):990–996
10. Fu P-f, Mao Z-y, Wang Y-j, Tang Z-y, Zuo C-j (2015) Fatigue properties of heavy-thickness Ti6.5Al2Zr1Mo1V alloy with oscillation EBW [J]. Vacuum 121:230–5
11. Li X, Hu S, Xiao J, Ji L (2011) Effects of the heterogeneity in the electron beam welded joint on fatigue crack growth in Ti–6Al–4V alloy [J]. Mater Sci Eng: A 529:170–176
12. Zhang Y, Wang H, Chen S, Hu G, Ouyang D, Cui X, Hu S (2022) Effect of heat treatment on microstructure and mechanical properties of laser solid forming TB18 titanium alloy [J]. Heat Treat Met 47:124–129
13. Zhou W, Liu XH, Feng J, Xin SW, Zhang SY, Zhang XQ, Wang T, Qin FY, Li B (2022) Grain growth kinetics of TB18 titanium alloy [J]. Rare Metal Mater Eng 51:3129–3132
14. Hu Z, Yuan W (2023) Finite element analysis for residual stress of TB18 billet produced by laser directed energy deposition [J]. Mater Res Express 10(3):036511
15. Li C, Zhang X, Zhou K et al (2012) Relationship between lamellar α evolution and flow behavior during isothermal deformation of Ti–5Al–5Mo–5V–1Cr–1Fe near β titanium alloy [J]. Mater Sci Eng: A 558:668–674
16. Wang K, Li MQ (2014) Effects of heat treatment and hot deformation on the secondary α phase evolution of TC8 titanium alloy [J]. Mater Sci Eng: A 613:209–216
17. Long J, Zhang L-J, Ning J, Ma Z-X, Zang S-L (2021) Zoning study on the fatigue crack propagation behaviors of a double-sided electron beam welded joint of TC4 titanium alloy with the thickness of 140 mm [J]. Int J Fatigue 146:106145
18. Long J, Zhang L-J, Zhang Q-B, Wang W-K, Zhong J, Zhang J-X (2020) Microstructural characteristics and low cycle fatigue properties at 230 °C of different weld zone materials from a 100 mm thick dissimilar weld of ultra-supercritical rotor steel [J]. Int J Fatigue 130:105248
19. Castany P, Besse M, Gloriant T (2012) In situ TEM study of dislocation slip in a metastable β titanium alloy [J]. Scripta Mater 66(6):371–373